DC Performances of ITER NbTi Conductors: Models vs. Measurements

D. Ciazynski, D. Bessette, P. Bruzzone, N. Martovetsky, B. Stepanov, R. Wesche, L. Zani, R. Zanino, and E. Zapretilina

***Abstract*—Within the R&D program on the International Thermonuclear Experimental Reactor (ITER) Poloidal Field (PF) coils, a full size conductor sample was tested in the SULTAN facility (CRPP Villigen, Switzerland). This sample is composed of two straight ITER-like cable-in-conduit conductors, using the same NbTi strand. The two conductors are identical except that one leg has a cable containing steel wraps around the main subcables as in the ITER design, while the other has no wraps inside. The paper presents conductor DC test results compared to predictions given by various models developed within ITER-associated laboratories. These models aim to predict the DC behavior of the cable from the experimental performances of the single strand. They have to explain the observed voltage-current (V-I) or voltage-temperature (V-T) characteristics, including the thermal runaways. The lower experimental performances compared to all expectations have shown the necessity to revise the models and to introduce a possible uneven current distribution among the strands of the cables.**

***Index Terms*—Cable-in-conduit, critical current, ITER, niobium titanium, PF coils.**

I. Introduction

WITHIN the R&D program on the ITER PF coils, a NbTi full size conductor sample (called PFIS) was tested in the SULTAN facility (CRPP, Villigen, Switzerland). In parallel to the fabrication of this sample [1] and to the preparation of the facility, several ITER-associated laboratories produced predictive analyzes based on the single strand experimental properties and their own models. They had to predict the whole conductor V-I and V-T characteristics, to be then compared to measurements. The lower experimental performances compared to all expectations have shown the necessity to revise the models by introducing an adjustable uneven current distribution among the strands of the cables in order to recover the measurements. The lower degradation (with respect to strand) of the conductors at low current has pleaded to include current redistribution phenomena in the models.

Manuscript received October 4, 2001.

D. Ciazynski and L. Zani are with the Euratom-CEA Association, CEA/DSM/DRFC, CEA/Cadarache, F-13108 Saint-Paul-lez-Durance, France (e-mail: daniel.ciazynski@cea.fr; louis.zani@cea.fr).

D. Bessette is with the ITER CTA, Max Plank Institute fur Plasmaphysik, Garching, Germany (e-mail: bessetd@itereu.de).

P. Bruzzone, B. Stepanov, and R. Wesche are with the Switzerland-Euratom Association, EPFL, CRPP-TF, Villigen, Switzerland (e-mail: pierluigi.bruzzone@psi.ch; boris.stepanov@psi.ch; rainer.wesche@psi.ch).

N. Martovetsky is with the Lawrence Livermore National Laboratory, Livermore, CA 94550 USA (e-mail: martovetsky1@llnl.gov).

R. Zanino is with the EPTO, Torino, Italy (e-mail: zanino@polito.it).

E. Zapretilina is with the NIIEFA (Efremov Institute), St. Petersburg, Russian Federation (e-mail: egorovsa@sintez.niiefa.spb.su).

Digital Object Identifier 10.1109/TASC.2005.849086

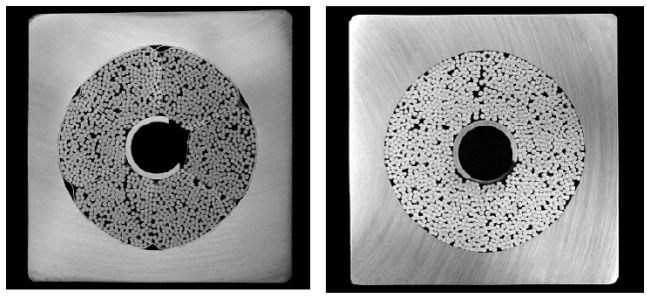

(a) (b)

Fig. 1. (a) Cross-section of PFIS left leg conductor (with wraps). (b). Cross-section of PFIS right leg conductor (w/o wraps).

II. Sample Description

The sample is composed of two parallel straight ITER-like cable-in-conduit conductors, joined at bottom through an overlap "praying-hand" joint. Details on the sample geometry and fabrication can be found in [1].

The two conductor legs are identical except that one leg has the regular ITER geometry with steel wraps around the last but one cabling stage (petal), while the other leg has no such wraps and thus requires a slightly higher compaction to keep the final void fractions equivalent [see Fig. 1(a) and (b)] [1], [2]. The conductor with wraps is identical to the one used in the fabrication of the ITER PF Coil Insert (PFCI) to be tested in the CSMC facility at JAERI, Naka (Japan) [3].

Both legs make use of the same NbTi strand, fabricated by Bochvar RIIM (Moscow, Russia). This strand is 0.73 mm in diameter, and has a copper noncopper ratio of 1.41 (average value over whole production). The cable contains 1440 strands which are twisted in a multistage cabling $(3 \times 4 \times 4 \times 5 \times 6)$. The cable final twist pitch is about 500 mm for both legs.

The conductor critical current is obtained by measuring the voltage drop V over 420 mm of conductor length (voltage taps on steel jacket) submitted to a uniform applied transverse field.

During experiment, the central channel is blocked in each leg, so that helium is flowing only through the annular (bundle) area. Temperature is measured just upstream of the high field length of each leg (sensor T5) [2].

III. Models Description

The aim of the models is to predict the V-I (or V-T) characteristics of the conductors using the measured properties of the strand composing their cables. This operation is not so simple due to the multi-twisting structure of the cable combined with the self-field produced by the two legs. As a matter of fact,

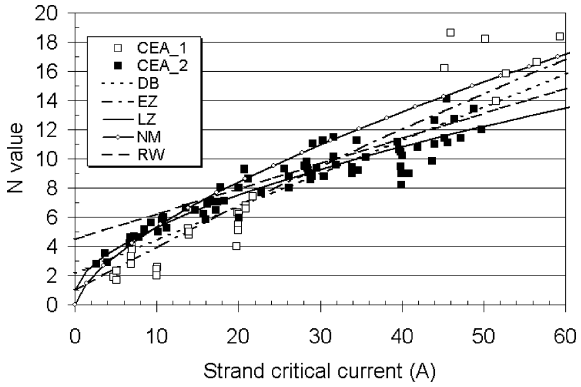

Fig. 2. PFIS strand n-value vs. critical current: $\mathrm{CEA\_1} + \mathrm{CEA\_2}$ = all experimental data, $\mathrm{CEA\_2}$ = selected data, and models.

for a transport current of 50 kA, the maximum self field on the cables is about 0.82 T, adding to the background field. The problem of the conductor stability has also to be addressed in these models. The test of the PFIS offered the opportunity to compare the models used by various ITER-associated laboratories, first between them, and then to experiment. In the following, the models will be referred using the initials of the authors of this paper (e.g. DB for D. Bessette).

A. Strand Properties

The strand NbTi critical current density is calculated using an interpolation formula provided by the supplier from all the data, marginally corrected by the testing group [2]. Other measurements were performed by CEA on one strand from the production [4]. The experimental n value data came from the CEA measurements but, due to a large scattering, all models did not use the same fits (see Fig. 2). Note that this scattering was later reduced by elimination of unreliable points (mainly coming indirectly from strand V-T measurements) [4].

B. Models Main Features

Most models assume uniform current distribution among strand, NM assume equal voltage between terminals which results in slightly different currents in the strands. All models consider "insulated" strands. The exercise turns then out to integrate the electric field all along the strands over 420 mm (or full length for NM model) and then to compute the mean among strands. The difficulty lies in the spatial variations of the magnetic field (known) and in the strand temperature (to be computed). Most models come from electro-magnetic models (DB [5], EZ [6], LZ [7], NM [8], RW [9]), one (RZ [10]) comes from a time dependent thermal-hydraulic model, although DB model also includes a one-fluid flow transient subroutine. Thus each model includes its own simplifications which may be then different among the models.

1) Magnetic Field: The majority (DB, EZ, LZ, RZ) uses the vector sum of the SULTAN field and of the sample self-field. Others (NM, RW) use approximate combinations.

2) Helium Temperature: Half (EZ, LZ, RW) considers helium temperature all along the 420 mm to be simply equal to the measured T5, whereas the others (DB, NM, RZ) compute it (averaged in cross-section) along conductor length.

3) Strand Temperature: Only one (LZ) considers it (not for stability) as equal to helium temperature, whereas the majority (DB, EZ, NM, RW, RZ) computes it through heat power balance with helium. The effective heat exchange coefficients taken in the models are rather scattered because empirical values are generally used: 400 $\mathrm{W/m^2/K}$ for NM, 700 for EZ, 1000 (with wraps) and 1500 (w/o wraps) for RW, 500 for RZ. Two (DB and LZ for stability) compute it from thermohydraulics but use different models and get different values: $\approx 400\,\mathrm{W/m^2/K}$ for DB [5], and $\approx$1800 for LZ [11].

4) Electric Field: Half (EZ, RW, RZ) computes an average value over the cable cross-section, whereas the others (DB, LZ, NM) integrate the electric field along the strand lengths and then perform an averaging over the strands. The latter is more accurate but requires to compute previously the strand trajectories in the cable [7]. Note that NM models only the last two cabling stages.

The majority (DB, EZ, LZ, NM, RW) computes strand electric field using the n value given in Fig. 2, applied to each individual strand, whereas only one (RZ) takes a constant n computed from Fig. 2 at the conductor critical current value. Only two models (DB and LZ) take into account the effect of the angle of the magnetic field with respect to the strand, with an anisotropy parameter $\mathrm{P} = 0.3$ [12]

5) Stability: Most of the models (EZ, LZ, NM, RW) compute the conductor stability through the heat balance of one single isolated strand experiencing the maximum electric field (i.e. located in the maximum magnetic field). Two models (DB, RZ) compute the overall conductor behavior and the instability appears then as a numerical runaway.

C. Discussion

It can be seen from the previous sections (III-B-1 to III-B-5) that no model is "perfect", all models make use of a few electromagnetic or thermal simplifications. Obviously, these simplifications are generally justified, but all in all, the results may be slightly different. They will be compared between them and with experimental results in the following section.

IV. Comparisons Between Models and Experiment

Because of the high Joule heating in the bottom joint [2], only V-T curves have been retained to perform comparisons between models and experiment.

A. Low Current V-T Characteristics

Below 30 kA, it was possible to record full V-T characteristics. Comparisons between predictions and experimental result at 20 kA under a 5 T field are presented in Fig. 3. It can be seen in this figure that all the models give a $\mathrm{T_{cs}}$ value ($\mathrm{V} = 4.2\,\mu\mathrm{V} \Leftrightarrow \mathrm{E} = 10\,\mu\mathrm{V/m}$) within 0.04 K. The experimental curve is first much higher in terms of voltage drop, and also more curved (i.e. a lower cable n value). Thus the experimental $\mathrm{T_{cs}}$ is about 0.14 K lower than the mean value of the predictions. A similar result is obtained on the left leg.

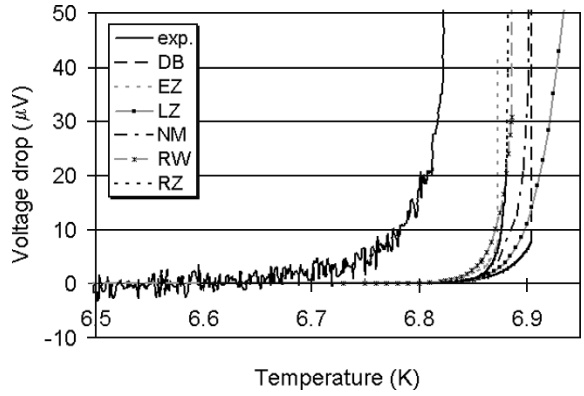

Fig. 3. Right leg voltage drop over 420 mm as function of temperature at 20 kA under a 5 T field: experiment (exp.) vs. models.

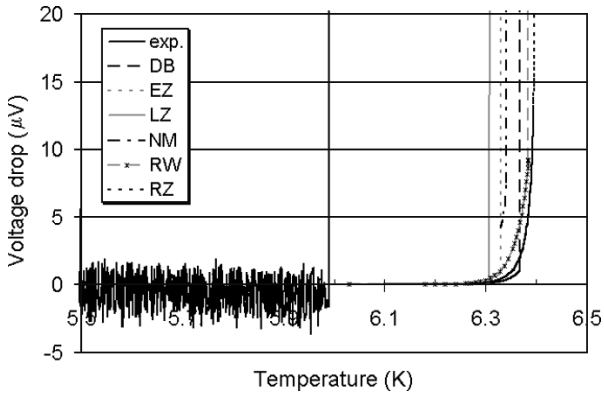

Fig. 4. Right leg voltage drop over 420 mm as function of temperature at 60 kA under a 5 T field: experiment (exp.) vs. models.

B. High Current V-T Characteristics

It was possible to measure a current sharing temperature on the right leg up to 45 kA at 5 T (the take off occurred then at about $\mathrm{V} = 5\ \mu\mathrm{V}$) and up to about 38 kA on the left leg (although not explored up to 42 kA). Under the same field, at 60 kA, no significant evolution of V could be observed before the take-off (see Fig. 4). For this run, the scattering among the predicted curves is larger than before, around 0.08 K. The measured quench temperature is about 0.35 K lower than the predictions (about 0.55 K in the left leg). Only one model (LZ) predicted a sharp take-off as observed, all the others predicted a measurable voltage drop (more or less high) before take-off. Clearly, this run is testing more the stability models than the regular V-T characteristics.

C. Conclusions

While the predicted performances are rather close, the performances of the two conductor legs are below all the expectations (i.e. outside the predicted ranges) regarding both critical currents and quench currents. The difference between experiment and predictions increases with sample current.

For understanding these results some corrections were made. First, to consider uncertainties on strand performances (see [4]), then to analyze the effect of a possible uneven current distribution among strands. Some models (DB, EZ, LZ) have been improved to take this into account.

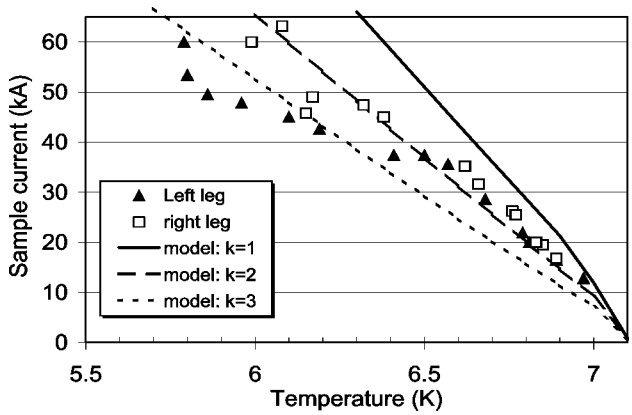

Fig. 5. Quench points on left and right legs under a 5 T field: experiment vs. (average) model with overload factor k.

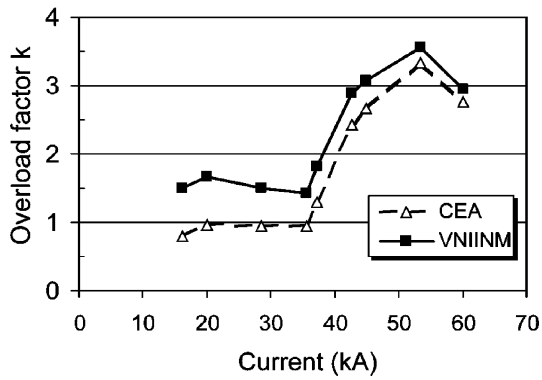

Fig. 6. Strand overload factor computed with EZ model on left leg under a 5 T field to fit experimental quench points, with CEA and VNIINM strand data.

V. Effect of Current Unbalance Among Strands

A. Strand Overload Factor

Considering an uneven current distribution among strands, one can check the stability of the most loaded strands, assuming an overload factor $\mathrm{k} > 1$ in current with respect to a uniform current distribution. This punctual operation does not oblige to depict the whole current distribution among the strands. In Fig. 5, the effect of k (average model) is presented compared to experimental quench points. It can be seen in this figure that the quench current is higher in the right (no wraps) leg. In order to explain the observed current limitation at low temperature one must consider $\mathrm{k} \approx 2$ in the right leg, and $\mathrm{k} \approx 3$ in the left leg. However, in doing so, one underestimates the quench current at higher temperature in both legs. Similar results are also obtained from measurements at 4 T and 6 T, with k slightly decreasing with magnetic field.

Therefore, one is led to consider a value of k increasing with sample current. This is particularly clear in Fig. 6 (from EZ model), in which the value of k required to recover experimental data has been plotted in function of current.

The effect of the strand properties (VNIINM and CEA data) is also shown in this figure. Note that values of k lower than 1 can be explained by the use of different strands in the cable and/or by the neglect of the strand/field angle in the EZ model.

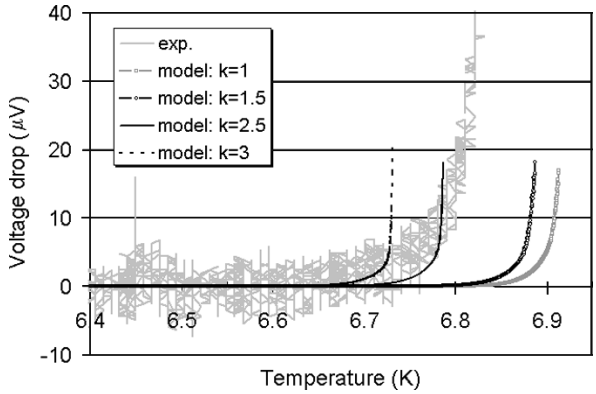

Fig. 7. Comparisons between experiment and model (DB) predictions with overloaded petals at 20 kA (right leg) under 5 T.

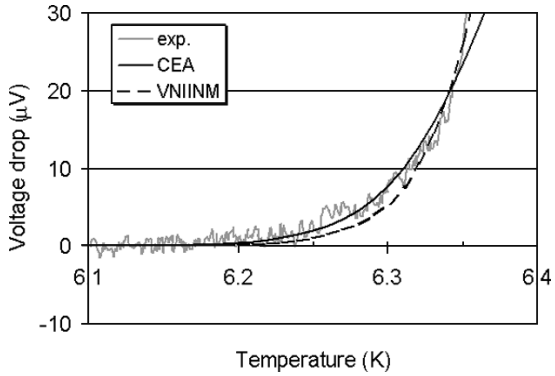

Fig. 8. Comparisons between experiment and model (LZ) predictions with overloaded petals and current redistribution at 20 kA (right leg) under 6 T.

B. Petal Overload Factor

The previous models offer the advantage of simple adaptations to existing models, but they do not give any idea of the origin of the nonuniformity and they also cannot predict full V-T characteristics and so critical currents. To go further, it is needed to impose an uneven current distribution among the strands; the simplest way is to consider nonuniformity among the main subcables (petals). One petal is then overloaded in current by a factor of k (DB model). This could result from fabrication problems in the lower joint of the sample which presented an unexpected high resistance [2]. Computed V-T characteristics are compared to experiment in Fig. 7 as function of k.

In order to recover the experimental quench temperatures at 5 T (with 20 kA, 45 kA, 60 kA), the value of k has to be adjusted within 2–2.5 for the right leg and within 2.5–3.3 for the left leg (VNIINM strand data). Note that slightly lower values of k are obtained using the CEA strand data. The general trend is to increase k with current. The weak point of this model is that it does not allow current redistribution among petals, particularly, it can be seen in Fig. 7 that the curvature of the V-T curve is not well predicted, the voltage development is more abrupt than observed experimentally.

C. Current Redistribution

As soon as a significant electric field appears along the overloaded petal, current can be transferred to less loaded petals, in the joints as well as along the conductor length. This phenomena can be modeled using an electrical network (LZ) [7]. A typical curve is shown in Fig. 8. The model can fit well the experimental V-T characteristics, using a realistic inter-petal resistance (i.e. 1 $\mu\Omega.\mathrm{m}$ for the wrapped cable, 0.2 $\mu\Omega.\mathrm{m}$ for the unwrapped cable).

In this model too, it is needed to consider an initial (at 4.5 K) uneven current distribution among petals. The overload factors are here 1.7 for the right leg and 2.2 for the left leg, using VNIIMN strand data, and 1.3 and 1.4 using the CEA strand data, respectively. However, with these factors, the model cannot predict the sudden take-offs observed at high currents, which are likely due to uneven current distribution among strands in the overloaded petal itself.

VI. Conclusions

The PFIS conductor performances have been found to be lower than expected by any models for both legs. Better predictions are obtained using the CEA strand data compared to the VNIINM data (i.e. using lower strand performances).

Dramatic current limitation (quench) can be explained by highly uneven current distribution among petals as well as among strands inside petals.

Uniformity can be improved by current redistribution among petals and strands which can explain the better stability of the unwrapped conductor leg and the better performances measured on both legs at low current. However, no model is presently capable to explain the full behavior of the PFIS conductors.

References

[1] F. Hurd *et al.*, "Design and manufacture of a full size joint sample (FSJS) for the qualification of the Poloidal Field (PF) insert coil," *IEEE Trans. Appl. Supercond.*, June 2005, to be published.

[2] P. Bruzzone *et al.*, "Test results of the ITER PF insert conductor short sample in SULTAN," *IEEE Trans. Appl. Supercond.*, June 2005, to be published.

[3] R. Zanino *et al.*, "Preparation of the ITER Poloidal Field Conductor Insert (PFCI) test," *IEEE Trans. Appl. Supercond.*, June 2005.

[4] L. Zani *et al.*, "Jc(B,T) characterization of NbTi strands used in ITER PF-relevant insert and full-scale sample," *IEEE Trans. Appl. Supercond.*, June 2005, to be published.

[5] D. Bessette, "Analysis of DC performance results of NbTi and Nb3Sn ITER relevant cable in conduit conductors," IEEE Trans. Appl. Supercond., June 2005, to be published.

[6] E. Zapretilina, "Analysis of Anomalous Behavior of V-I Characteristic With 'Bumps'," CRPP Internal Report, Feb. 2004.

[7] T. Schild, D. Ciazynski, and S. Court, "Effect of actual cabling pattern on the critical current of a multistage CICC," *Adv. in Cryo. Eng.*, vol. 46B, p. 1051, 2000.

[8] N. Martovetsky, "Trying to predict NbTi PFIS in SULTAN," in PFIS Test Group Meeting, Cadarache, Mar. 12, 2004.

[9] R. Wesche *et al.*, "DC performance of subsize NbTi cable-in-conduit conductors," *IEEE Trans. Appl. Supercond.*, vol. 14, pp. 1499–1502, 2004.

[10] R. Zanino *et al.*, "A two-fluid code for the thermohydraulic transient analysis of CICC superconducting magnets," *J. Fus. Energy*, vol. 14, pp. 25–40, 1995.

[11] S. Nicollet *et al.*, "Evaluation of the ITER cable-in-conduit conductor heat transfer," presented at the 20th Int. Cryo. Eng. Conf., Beijing, 2004.

[12] S. Takacs *et al.*, "Critical currents of NbTi tapes with differently oriented anisotropic defect," *Cryogenics*, pp. 153–159, Mar. 1983.